A&A 589, A78 (2016)
DOI: 10.1051/0004-6361/201528041

Astronomy & Astrophysics

Isotopic ratios of H, C, N, O, and S in comets C/2012 F6 (Lemmon) and C/2014 Q2 (Lovejoy)⋆,⋆⋆,⋆⋆⋆

N. Biver[1], R. Moreno[1], D. Bockelée-Morvan[1], Aa. Sandqvist[2], P. Colom[1], J. Crovisier[1], D. C. Lis[3], J. Boissier[4], V. Debout[1], G. Paubert[5], S. Milam[6], A. Hjalmarson[7], S. Lundin[8], T. Karlsson[8], M. Battelino[8], U. Frisk[9], D. Murtagh[10], and the Odin team.

[1] LESIA, Observatoire de Paris, PSL Research University, CNRS, Sorbonne Universités, UPMC Univ. Paris 06, Univ. Paris Diderot, Sorbonne Paris Cité, 5 place Jules Janssen, 92195 Meudon, France
e-mail: nicolas.biver@obspm.fr
[2] Stockholm Observatory, AlbaNova University Center, 106 91 Stockholm, Sweden
[3] LERMA, Observatoire de Paris, PSL Research University, CNRS, Sorbonne Universités, UPMC Univ. Paris 06, 75014 Paris, France
[4] IRAM, 300, rue de la Piscine, 38406 Saint-Martin-d'Hères, France
[5] IRAM, Avd. Divina Pastora, 7, 18012 Granada, Spain
[6] NASA Goddard Space Flight Center, Astrochemistry Laboratory, Code 691.0, Greenbelt, MD 20771, USA
[7] Onsala Space Observatory, Chalmers University of Technology, 439 92 ONSALA, Sweden
[8] OHB Sweden, PO Box 1269, 164 29 Kista, Sweden
[9] Omnisys Instruments, August Barks Gata 6B, 421 32 Västra Frölunda, Sweden
[10] Dept. of Radio and Space Science, Chalmers Technical University, 41258 Gothenburg, Sweden

Received 24 December 2015 / Accepted 4 March 2016

ABSTRACT

The apparition of bright comets C/2012 F6 (Lemmon) and C/2014 Q2 (Lovejoy) in March-April 2013 and January 2015, combined with the improved observational capabilities of submillimeter facilities, offered an opportunity to carry out sensitive compositional and isotopic studies of the volatiles in their coma. We observed comet Lovejoy with the IRAM 30 m telescope between 13 and 26 January 2015, and with the *Odin* submillimeter space observatory on 29 January–3 February 2015. We detected 22 molecules and several isotopologues. The $H_2^{16}O$ and $H_2^{18}O$ production rates measured with *Odin* follow a periodic pattern with a period of 0.94 days and an amplitude of ~25%. The inferred isotope ratios in comet Lovejoy are $^{16}O/^{18}O = 499 \pm 24$ and $D/H = 1.4 \pm 0.4 \times 10^{-4}$ in water, $^{32}S/^{34}S = 24.7 \pm 3.5$ in CS, all compatible with terrestrial values. The ratio $^{12}C/^{13}C = 109 \pm 14$ in HCN is marginally higher than terrestrial and $^{14}N/^{15}N = 145 \pm 12$ in HCN is half the Earth ratio. Several upper limits for D/H or $^{12}C/^{13}C$ in other molecules are reported. From our observation of HDO in comet C/2014 Q2 (Lovejoy), we report the first D/H ratio in an Oort Cloud comet that is not larger than the terrestrial value. On the other hand, the observation of the same HDO line in the other Oort-cloud comet, C/2012 F6 (Lemmon), suggests a D/H value four times higher. Given the previous measurements of D/H in cometary water, this illustrates that a diversity in the D/H ratio and in the chemical composition, is present even within the same dynamical group of comets, suggesting that current dynamical groups contain comets formed at very different places or times in the early solar system.

Key words. radio lines: planetary systems – submillimeter: planetary systems – comets: individual: C/2012 F6 (Lemmon) – comets: individual: C/2014 Q2 (Lovejoy) – comets: general

1. Introduction

Comets are the most pristine remnants of the formation of the solar system 4.6 billion years ago. Investigating the composition of cometary ices provides clues to the physical conditions and chemical processes at play in the primitive solar nebula. Comets may also have played a role in the delivery of water and organic material to the early Earth (see Hartogh et al. 2011, and references therein). The latest simulations of the early solar system evolution (Brasser & Morbidelli 2013; O'Brien et al. 2014), suggest a more complex scenario. On the one hand, ice-rich bodies formed beyond Jupiter may have been implanted in the outer asteroid belt and participated in the supply of water to the Earth or, on the other hand, current comets coming from either the Oort Cloud or the scattered disk of the Kuiper belt may have formed in the same trans-Neptunian region sampling the same diversity of formation conditions. Understanding the diversity in composition and isotopic ratios of the comet material is thus essential in order to assess such scenarios (Altwegg & Bockelée-Morvan 2003; Bockelée-Morvan et al. 2015).

The recent years have seen significant improvement in the sensitivity and spectral coverage of millimeter receivers. The EMIR receivers (Carter et al. 2012) at the Institut de radioastronomie millimétrique (IRAM) are equipped with a fast

⋆ Based on observations carried out with the IRAM 30 m telescope. IRAM is supported by INSU/CNRS (France), MPG (Germany) and IGN (Spain).
⋆⋆ *Odin* is a Swedish-led satellite project funded jointly by the Swedish National Space Board (SNSB), the Canadian Space Agency (CSA), the National Technology Agency of Finland (Tekes) and the Centre National d'Études Spatiales (CNES, France). The Swedish Space Corporation is the prime contractor, also responsible for *Odin* operations.
⋆⋆⋆ The spectra dataset is only available at the CDS via anonymous ftp to cdsarc.u-strasbg.fr (130.79.128.5) or via http://cdsarc.u-strasbg.fr/viz-bin/qcat?J/A+A/589/A78

Fourier transform spectrometer that offers a wide frequency coverage at a high spectral resolution (0.2 MHz). The combination enables sensitive spectral surveys of cometary atmospheres and simultaneous observations of several molecules, including isotopologues in brighter comets. We report here observations of isotopic ratios with the IRAM 30 m radio telescope in two very active (maximum water outgassing rate close to 10^{30} molec s^{-1}) Oort cloud comets, C/2012 F6 (Lemmon) and C/2014 Q2 (Lovejoy), carried out in 2013 and 2015. They are both dynamically old Oort cloud comets: an original orbital period of 9800 years and an orbit inclination of 83° for comet Lemmon, and a period of 11 000 years and an inclination of 80° for comet Lovejoy.

The analysis of the observation in terms of molecular abundances and detection of rare and new molecular species has been reported (Biver et al. 2014, 2015). In the present article we concentrate on the measurement of several isotopic ratios. We report the detection of HDO in both comets. The compounds $H_2^{16}O$ and $H_2^{18}O$ were detected in comet Lovejoy with the *Odin* submillimeter space observatory, which helped to accurately determine the D/H and $^{16}O/^{18}O$ ratio in water in this comet.

2. Observations

2.1. IRAM Observations

Comet C/2014 Q2 (Lovejoy) was observed with the IRAM 30 m radio telescope during two periods: on 13.8, 15.8, and 16.8 January 2015 (geocentric distance Δ = 0.496–0.528 AU) and on 23.7, 24.7, 25.7, and 26.7 January 2015 (Δ = 0.624–0.675 AU) under very good weather conditions. The heliocentric distances were 1.31 and 1.29 AU, respectively. Perihelion was on 30.07 January UT, at 1.290 AU from the Sun. The 13–25 and 26 January observations were conducted with the EMIR 1 mm and 3 mm receivers, respectively. The main backend used is a Fourier transform spectrometer, which covers a frequency range of 2 × 8 GHz (two sidebands separated by 8 GHz, each in two linear polarizations) in a single setup, with a high spectral resolution of 200 kHz. The spectral resolution (0.3–0.2 km s^{-1} when converted into Doppler velocity) allows the velocity profiles of the narrow cometary lines (~2 km s^{-1}) to be resolved. We also used the high resolution VESPA autocorrelator set to 40 kHz sampling on dedicated lines of interest (e.g., CH_3OH ($5_{+2} - 4_{+1}E$) and $H^{15}CN$ (3–2)), but VESPA units can only cover lines within a 0.5 GHz window centered at 6.25 GHz in the IF band (upper and lower side band). Using four different tunings we covered the 210–218, 225–233, and 240–272 GHz frequency ranges and 85–93 and 101–109 GHz.

The half power beam width of the IRAM 30 m telescope in the 1 mm band ranges from 9.1″ to 11.6″, which corresponds to 3300 to 5400 km at the comet distance (22–28″ at 3 mm corresponding to 11 000–14 000 km on 26.7 Jan.). Given the expansion velocity of the coma (~0.8 km s^{-1}) and heliocentric distance, this means that we are not very sensitive to the photodissociation rate of the molecules, provided that the molecule lifetime at 1 AU is larger than 4000 s. The pointing accuracy (1″–2″) was regularly checked on reference pointing sources and also on the comet with coarse maps. The time variation of the activity of the comet could be monitored with the multiple strong CH_3OH lines present in all setups. We did not see any variations significantly larger than ±20% during the observations (Q_{CH_3OH} = 1.2 ± 0.2 × 10^{28} molec s^{-1}, 13–16 January, and 1.4 ± 0.2 × 10^{28} molec s^{-1}, 23–25 January), which justified the averaging of several days of observations.

Comet C/2012 F6 (Lemmon) was observed in March and April 2013 (as already presented in Biver et al. 2014). Perihelion was on 24.51 March 2013 UT at 0.731 AU from the Sun. We mostly used the same tunings as for comet Lovejoy with the EMIR 1mm receiver combined with the FTS and VESPA spectrometers. The best weather conditions were found on 14.5 and 18.5 March, but with a comet at low elevation (15–20°), and on 6.5 April 2013. We covered the 240–272 GHz frequency range and obtained noisier data on the 85–93, 166–170, and 210–242 GHz bands with the EMIR 3 mm, 2 mm, and 1 mm receivers, respectively. A summary of the observational setups is given in Table A.1.

In this paper we focus only on the measurement of isotopic ratios, and spectra of isotopologues are presented in Figs. 3–8. The chemical inventory of these comets based on these observations with the IRAM telescope has been presented in Biver et al. (2014, 2015) and will be further detailed in a future paper.

2.2. Odin observations of comet C/2014 Q2 (Lovejoy)

Because comet C/2014 Q2 (Lovejoy) clearly became a very active comet, observations with the *Odin* 1.1 m submillimeter satellite (Frisk et al. 2003) were triggered on a late notice. Observations took place between 30.5 January and 3.4 February 2015. These observations were scheduled to map the emission of $H_2^{16}O$ at 556.9 GHz, follow its temporal evolution, and detect the $H_2^{18}O$ line at 547.7 GHz. The half power beamwidth is close to 2.1′ at these frequencies and the main beam efficiency is 0.89. *Odin* uses three spectrometers: a 1 GHz bandwidth acousto-optical spectrometer (AOS with 0.6 MHz sampling) and two autocorrelators (AC1 and AC2) used in their highest resolution mode (~0.15 MHz with 100 MHz bandwidth). For the first setup, two receivers tuned to the $H_2^{16}O$ line were used in parallel, coupled to the three spectrometers: AOS and AC2 on receiver 555-B2 and AC1 on 549-A1. For the second setup, the AOS was connected to the 572-B1 receiver tuned near the ammonia line at 572.5 GHz, but not frequency locked, while AC2 was connected to the receiver 555-B2 and AC1 to 549-A1, both tuned to the $H_2^{18}O$ line.

As *Odin* is in a helio-synchronous polar Earth orbit at 550 km altitude, the comet was only observable during ~55 min of each 96 min orbit. The Earth was in the field of view during the remaining time, and the atmospheric lines were used to calibrate the frequency scale. Some of the observations failed to track the comet correctly, but half were successful and provided good results. Spectra of the nucleus-centered $H_2^{16}O$ and $H_2^{18}O$ lines are shown in Fig. 3 and a map of the $H_2^{16}O$ line is shown in Fig. 1.

3. Modeling of the lines and model parameters

3.1. Velocity and outgassing pattern

The mean gas expansion velocity was derived from the shape of the lines with the highest signal-to-noise ratio. We determined a value of 1.1 to 1.0 km s^{-1} for comet Lemmon and 0.8 km s^{-1} for comet Lovejoy (Table A.1). As discussed hereafter, comet Lovejoy was observed with the larger beam of *Odin*; a value of 0.85 km s^{-1} provided a better fit to the width of the water lines. This is expected, as acceleration of the gas expansion velocity in the coma is predicted and observed in the outer part of the comae of active comets.

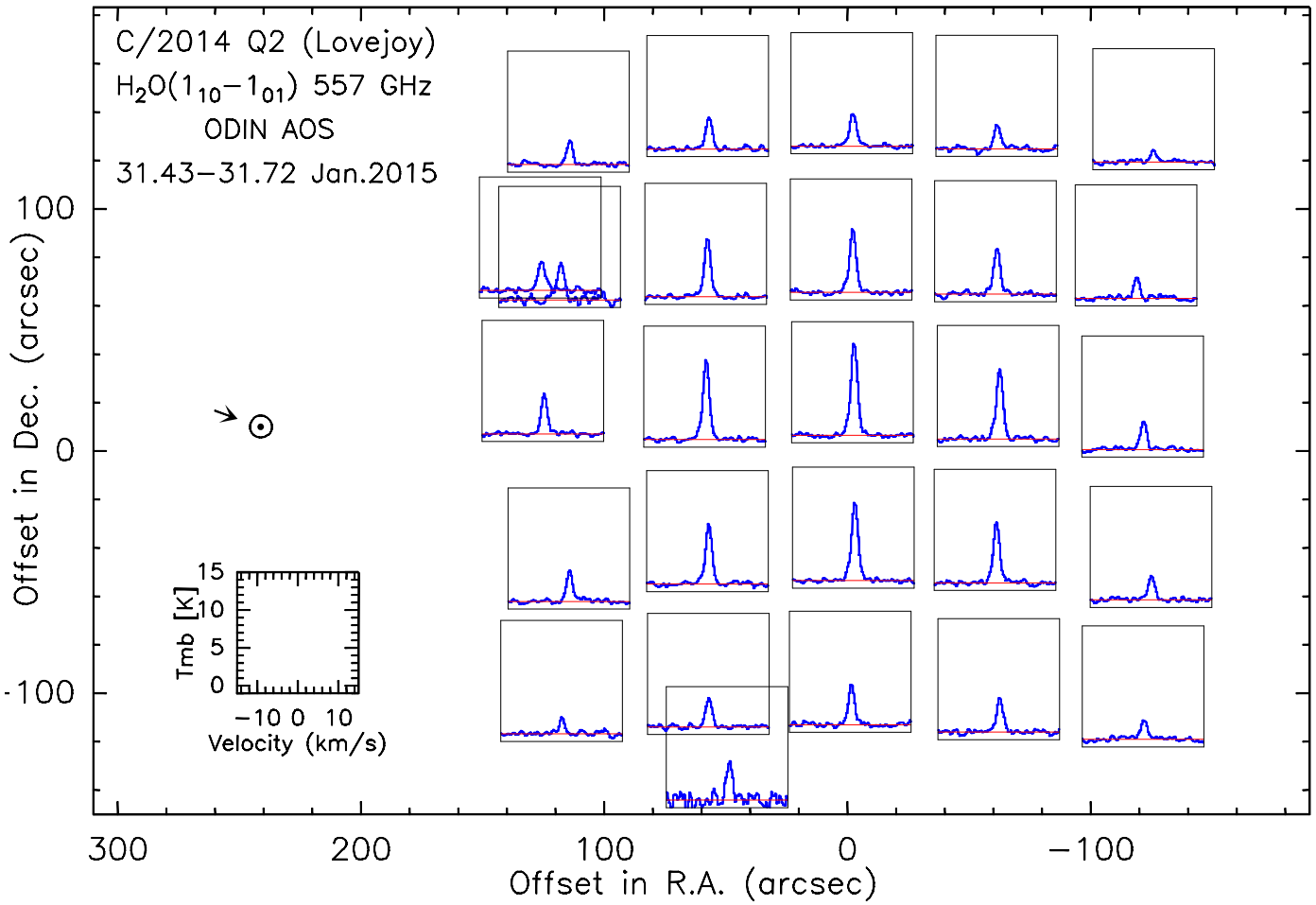

Fig. 1. Map of the $H_2^{16}O$ $(1_{10}-1_{01})$ line obtained with *Odin* and its acousto-optical spectrometer in comet Lovejoy. The arrow provides the projected direction of the Sun (phase angle was 50°), but the water emission does not exhibit any significant asymmetry.

3.2. Temperature and collisional excitation

For all molecules we used the latest spectroscopic data available in the JPL (Pickett et al. 1998) and CDMS (Müller et al. 2005) databases, both for line identification and computation of line strengths. We employed the code previously used for other comets (Biver et al. 2007; Hartogh et al. 2011; Bockelée-Morvan et al. 2012) to compute the excitation of the rotational levels of the molecules and the line intensities. We take into account the pumping of the rotational levels by the fluorescence of the infrared vibrational bands, which is not expected to play a major role at the cometocentric distances ≤5000 km sampled in the case of comet Lovejoy. In our model molecules slowly evolve from the local thermal equilibrium (T = 100−110 and 73 K, for comets Lemmon and Lovejoy, respectively; Table A.1) maintained by collisions with neutrals and electrons close to the nucleus to spontaneous decay of the rotational population in the less dense parts of the coma (Biver et al. 2000, 2006). Within the accuracy of the detections, line intensity ratios (or rotational temperatures) for methanol, and also for most other species, are in agreement with the model (e.g., $T_{\rm rot}(CH_3CHO, \text{Lovejoy})$ = 67 ± 15 K for 68 K predicted). The density is described with the Haser model, using lifetimes from Crovisier (1994), Bockelée-Morvan et al. (2000), and Crovisier et al. (2004a,b). Line intensities are computed with a radiative transfer code that takes opacity effects into account. Except for $H_2^{16}O$ and HCN, lines are optically thin, meaning that line intensities are proportional to the production rates.

4. Water production rate and time evolution

4.1. Odin maps and excitation of water in the coma of comet Lovejoy

Several maps (e.g., Fig. 1) of the water emission were performed for comet Lovejoy with *Odin* in order to precisely derive the water production rate. The extension of the emission of optically thick submillimeter water lines in cometary comae is in large part governed by the excitation mechanism of the water rotational levels. It depends both on the temperature profile and collision rates with electrons and neutrals in the inner part of the coma (Biver et al. 2007; Hartogh et al. 2011; Bockelée-Morvan et al. 2012). However, in the outer part (beyond 150″) the line intensity mostly depends on the water production rate (and assumed photo-dissociation lifetime), and very little on the assumed temperature profile. Dividing the gas temperature by a factor of 2 only increases the derived production rate by 10%. We used the same excitation parameters for the $H_2^{16}O$ observations with *Odin*, as those derived for the molecular lines observed with the IRAM 30 m instrument: a constant temperature of 73 K throughout the coma and an electron density scaling factor $x_{\rm ne}$ = 0.5 (Zakharov et al. 2007; Biver et al. 2007). The expansion velocity inferred from the $H_2^{16}O$ and $H_2^{18}O$ line widths is $v_{\rm exp}$ = 0.85 km s^{-1}, slightly

Table 1. Periodic variation of water production in comet Lovejoy.

Odin measurements 29 January–3 February 2015, r_h = 1.29 AU						
Data points	Molecule	Production rate variation fitted[a]				χ^2_ν
		Q_0	ΔQ	T_p	T_0	
		[10^{27} molec s^{-1}]		[days]	[UT day]	
23[b]	$H_2^{16}O$	751.6 ± 29.5	140 ± 21	0.938 ± 0.014	31.797 ± 0.038-Jan.	1.03
23[b]	$H_2^{16}O$	724.4 ± 14.6	141 ± 22	0.935[d]	31.742-Jan.[d]	1.09
23[b]	$H_2^{16}O$	774.0 ± 12.4	0.0[c]	–	–	2.78
15	$H_2^{18}O$	1.524 ± 0.065	0.374 ± 0.085	0.922 ± 0.031	31.400 ± 0.035-Jan.	1.21
15[b]	$H_2^{18}O$	1.453 ± 0.062	0.314 ± 0.083	0.935[d]	31.742-Jan.[d]	1.23
15	$H_2^{18}O$	1.421 ± 0.055	0.0[c]	–	–	2.44
38[b]	$H_2^{16}O$, $H_2^{18}O$[e]	724 ± 17	147 ± 19	0.939 ± 0.013	31.912 ± 0.022-Jan.	1.00

Notes. [(a)] $Q = Q_0 + \Delta Q \times \sin(2\pi(t - T_0)/T_p)$, where T_p is the period in days of the fitted sine variation and T_0 the reference time for the phase. [(b)] Including 5% uncertainty due to a 10″ pointing uncertainty. [(c)] Fit of constant production. [(d)] fixed value (see text). [(e)] Assuming $H_2^{16}O/H_2^{18}O$ = 500.

larger than for the lines observed with the smaller beam of the IRAM 30 m telescope. The fit to the radial profile of the line intensity from the map (Fig. 1) is satisfactory and corresponds to $Q_{H_2O} = 8.7 \pm 0.7 \times 10^{29}$ molec s^{-1}and the reduced $\chi^2_\nu = 2.4$ when we include the 5% uncertainty due to the 10″ (Frisk et al. 2003) pointing uncertainty. Taking into account an increase in the velocity with distance from the nucleus does not significantly change the goodness of the fit and the derived production rate.

4.2. Periodic variation in $H_2^{16}O$ and $H_2^{18}O$ production rates

Since $H_2^{16}O$ and $H_2^{18}O$ measurements with *Odin* were not simultaneous, but interlaced, in order to derive an accurate $H_2^{16}O/H_2^{18}O$ production rate ratio it is necessary to determine if significant short-time variation of the activity is present. Inspection of production rates does suggest that time variation is present in the data. Since the observations of $H_2^{18}O$ constituted a series of ten successive *Odin* orbits, we did a time averaging of ≈2.5 h, corresponding to two consecutive orbits of observations, yielding a sufficient signal-to-noise ratio (5−10) to look for time variations. We fitted a sinusoidal time variation to the individual measurements of the production rates of $H_2^{16}O$ and $H_2^{18}O$, independently. We only selected the $H_2^{16}O$ measurements with pointing offsets less than ∼100″. The results are provided in Table 1. For both molecules, the sinusoidal fit is better than assuming no time variation (χ^2_ν reduced by a factor ∼2.5), and the inferred period is similar (T_p = 0.922−0.940 day). A simulation of periodic variations of the production rates anticipated a longer delay between peak outgassing and peak signal for $H_2^{16}O$ than $H_2^{18}O$ (0.25 versus 0.14 day), which we took into account. We found different reference times T_0 for $H_2^{16}O$ and $H_2^{18}O$, but these are strongly correlated to the T_p value. Formally, the T_p-independent 1σ uncertainty δT_0 is on the order of 0.4 days. We also tried to fit the data with the same time dependence for $H_2^{16}O$ and $H_2^{18}O$, using a fixed mean period of T_p = 0.935 days (weighted average) and a corresponding reference time 31.742 Jan. 2015 UT. The goodness of the fits is similar (Table 1). A larger damping of the apparent production rate amplitude was expected for $H_2^{16}O$ due to optical depth effects. From the observations the effect is not so obvious: $\Delta Q/Q_0$ is only slightly smaller for $H_2^{16}O$ than for $H_2^{18}O$ (0.19 versus 0.24). We did not investigate the possible variation of the gas temperature with the production rate, but this could explain a variation of the line intensity with time that was larger than anticipated.

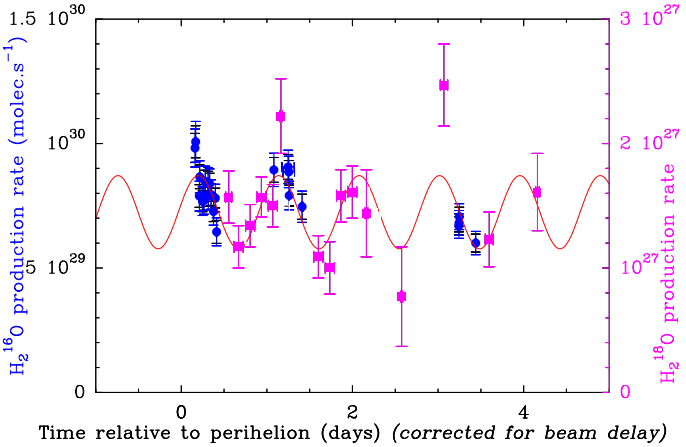

Fig. 2. $H_2^{16}O$ (left vertical scale) and $H_2^{18}O$ (pink, right vertical scale) production rates in comet Lovejoy from *Odin* observations. Horizontal scale is the time relative to perihelion (30.069 January 2015 UT) in days, minus the expected delay between peak outgassing and peak intensity due to beam dilution and opacity effect for a periodic outgassing with similar periodicity. Production rates are apparent production rates computed in the stationary regime assumption. For $H_2^{16}O$ the larger error bar includes a 5% uncertainty due to the 10″ pointing uncertainty. $H_2^{18}O$ uncertainty is dominated by statistical noise. The least square fit to the combined production rate (last line of Table 1) is overplotted.

We then combined both $Q_{H_2^{16}O}$ and $Q_{H_2^{18}O}$ to derive our best estimate of the water production rate as a function of time during the period 30 January to 3 February 2015 (last line of Table 1). Figure 2 shows the time evolution of the production rates measured for the two water isotopologues and best fit.

4.3. Reference water production rates

The reference water production rates were primarily derived from contemporaneous observations of the OH radical maser lines at 18 cm with the Nançay radio telescope. During the 12.8−16.8 January 2015 observing period of comet Lovejoy, both observations centered on the comet and at 3.0′ offset position were used to better constrain the quenching of the

Table 2. Isotopic ratios in comet C/2014 Q2 and C/2012 F6.

Isotopic ratio	Molecule	Value
Comet C/2012 F6 (Lemmon) Mar.-Apr. 2013		
D/H	H_2O	$6.5 \pm 1.6 \times 10^{-4}$
	HCN	<0.045
$^{12}C/^{13}C$	HCN	124 ± 64 or $\geq 89^b$
$^{14}N/^{15}N$	HCN	152 ± 72 or $\geq 106^b$
$^{32}S/^{34}S$	CS	20 ± 5
	H_2S	>3.5
Comet C/2014 Q2 (Lovejoy) Jan. 2015		
D/H	H_2O	$1.4 \pm 0.4 \times 10^{-4}$
	HCN	<0.006
	H_2S	<0.017
	H_2CO	<0.007
$^{12}C/^{13}C$	HCN	109 ± 14
	CH_3OH	>61
$^{14}N/^{15}N$	HCN	145 ± 12
$^{16}O/^{18}O$	H_2O	499 ± 24^a
$^{32}S/^{34}S$	CS	24.7 ± 3.5
	H_2S	>7
$^{32}S/^{33}S$	CS	>50

Notes. [a] From time variable fits of the production rates. [b] Based only on the backends with the lowest noise.

maser inversion (Gerard et al. 1998) yielding an average water production rate $Q_{H_2O} = 5.0 \pm 0.2 \times 10^{29}$ molec s^{-1} (Biver et al. 2015). For other periods and for comet Lemmon, the observations of the OH radical could not be used to derive an accurate water production rate owing to significant uncertainties in the quenching of the maser inversion. We either used the water production rates reported elsewhere (Combi et al. 2014; Paganini et al. 2014) or made an interpolation from the *Odin* observations of comet Lovejoy at perihelion. Based on Nançay and *Odin* observations, we adopt a mean Q_{H_2O} = 5, 5.5, 6, and 7×10^{29} molec s^{-1} for the 13–16 January, 13–25 January, 23–25 January, and 26 January–3 February 2015 time intervals, respectively, with a ±20% time variation possible within each time interval. Observations done on a short time interval might be affected by a periodic time variation, but this was tracked from the monitoring of the methanol production lines, which are present in all IRAM observations settings (Table A.1).

5. Isotopic ratios

Table A.2 provides the list of molecular lines (main species and isotopologues) observed at IRAM in comets C/2012 F6 (Lemmon) in 2013 and in C/2014 Q2 (Lovejoy) in 2015 and considered in this study. Line intensities and production rates (or upper limits) derived using the models presented in Sect. 3 are given. The corresponding isotopic ratios or 3σ limits are presented in Table 2.

5.1. $^{16}O/^{18}O$ ratio in comet Lovejoy

The analysis of *Odin* observations in Sect. 4.2 (Table 1) enabled us to derive an accurate $H_2^{16}O$ /$H_2^{18}O$ production rate ratio. From the sinusoidal fits and derived mean Q_0 production rates, we obtain:

- $Q_0(H_2^{16}O)/Q_0(H_2^{18}O) = 493 \pm 29$ for the independent fits;
- $Q_0(H_2^{16}O)/Q_0(H_2^{18}O) = 499 \pm 24$ for the phased fits.

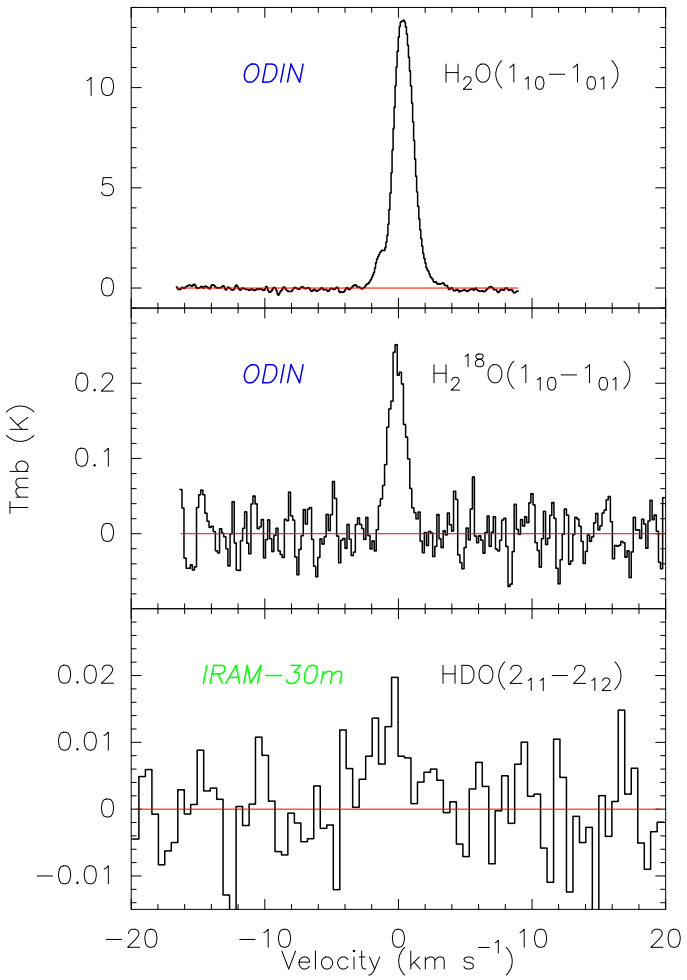

Fig. 3. Comet C/2014 Q2 (Lovejoy): average on-nucleus spectra of the $H_2^{16}O$ $(1_{10}-1_{01})$ line at 556.936 GHz, and $H_2^{18}O$ $(1_{10}-1_{01})$ line at 547.676 GHz obtained with *Odin* between 30 January and 3 February 2015. The spectrum of the HDO $(2_{11}-2_{12})$ line at 241.561 GHz observed with the IRAM 30 m telescope on 13–24 January 2015 is shown below. While the $H_2^{18}O$ and HDO lines are marginally blue-shifted ($\Delta v = -0.07$ km s^{-1} in both cases) the $H_2^{16}O$ $(1_{10}-1_{01})$ line is asymmetric and red-shifted ($\Delta v = +0.33$ km s^{-1}) due to self absorption by the cool gas in the foreground of this optically thick line. Vertical scale is main beam brightness temperature and horizontal scale Doppler velocity in the comet rest frame.

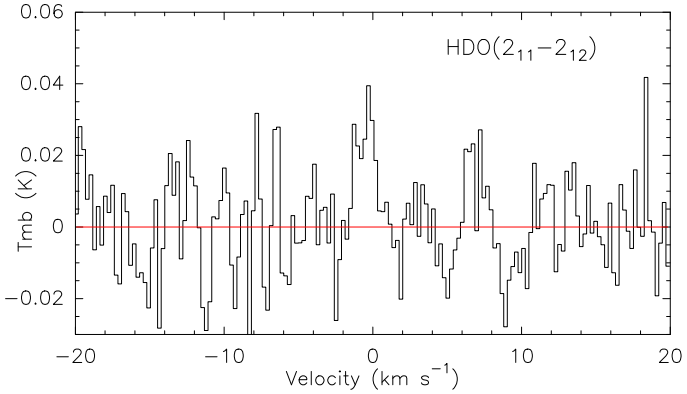

Fig. 4. Comet C/2012 F6 (Lemmon): average on-nucleus spectrum of the HDO $(2_{11}-2_{12})$ line at 241.561 GHz observed with the IRAM 30 m telescope between 14 March and 8 April 2013. Vertical scale is main beam brightness temperature and horizontal scale Doppler velocity in the comet rest frame.

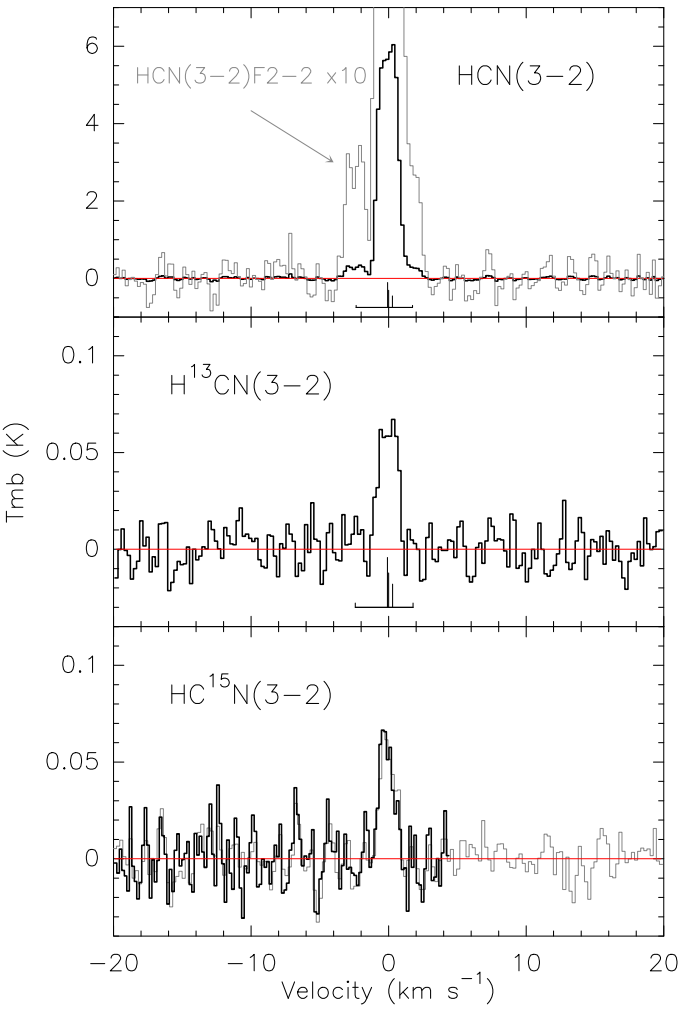

Fig. 5. Comet C/2014 Q2 (Lovejoy): average on-nucleus spectra of the HCN (3−2) line at 265.886 GHz, $H^{13}CN$ (3−2) line at 259.012 GHz, and $HC^{15}N$ (3−2) line at 258.157 GHz obtained with the IRAM 30 m telescope on 13–24 January 2015. For $HC^{15}N$ (3−2) the spectrum obtained with the VESPA autocorrelator (thick line) is superimposed on the FTS spectrum. Vertical scale is main beam brightness temperature and horizontal scale Doppler velocity in the comet rest frame.

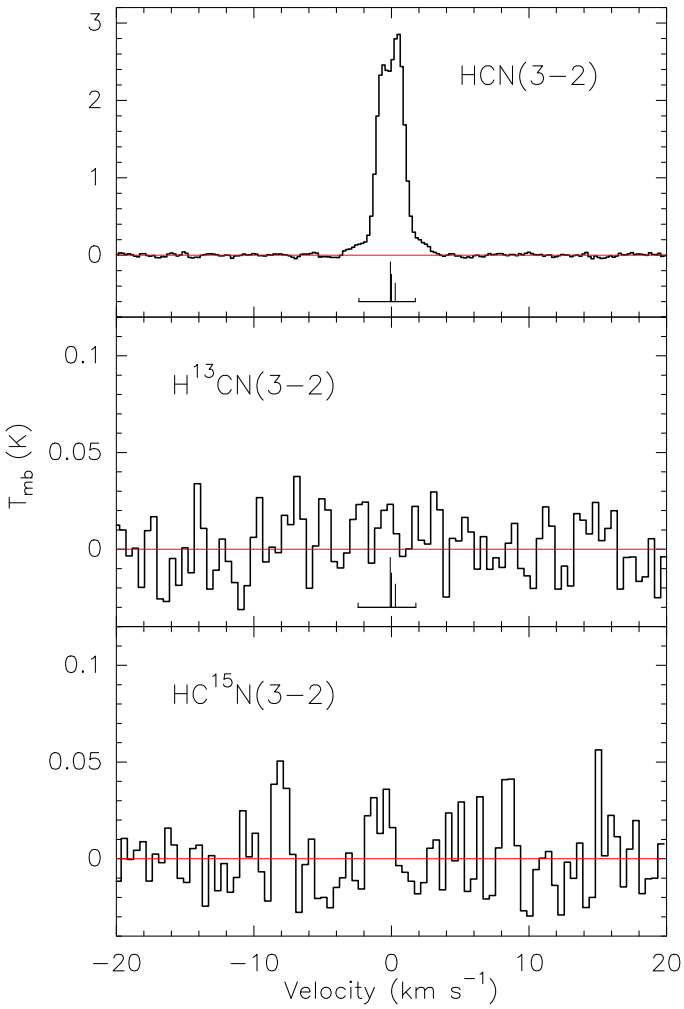

Fig. 6. Comet C/2012 F6 (Lemmon): average on-nucleus spectrum of the HCN (3−2) line at 265.886 GHz obtained with the IRAM 30 m telescope between 14 March and 8 April 2013. Spectra covering the same velocity range obtained at similar times for $H^{13}CN$ (3−2) (259.012 GHz) and $HC^{15}N$ (3−2) (258.157 GHz) are also shown for comparison, but do not show a clear detection. Vertical scale is main beam brightness temperature and horizontal scale Doppler velocity in the comet rest frame.

The second approach, which corresponds to a $H_2^{16}O$ /$H_2^{18}O$ ratio that does not vary with time, yields $^{16}O/^{18}O = 499 \pm 24$, which is exactly the terrestrial value (498.7).

5.2. D/H ratio

Thanks to the wide frequency coverage of IRAM observations, lines of deuterated species of known cometary molecules were observed. None were detected except the HDO (2_{11}−2_{12}) line at 241.562 GHz (Fig. 3). This is not surprising as water is over a hundred times more abundant than HCN, H_2S, or H_2CO. Nevertheless, the upper limits on the D/H ratio in H_2S or H_2CO in comet Lovejoy are the lowest obtained so far in a comet.

5.2.1. D/H ratio in water in comet C/2012 F6 (Lemmon)

We observed the HDO (2_{11}−2_{12}) line at 241.561 GHz in comet C/2012 F6 (Lemmon) in March-April 2013. The detection of HDO (Fig. 4) is also marginal (4σ) and the retrieved intensity was possibly affected by poorer baselines on 8 April when we could not use the telescope wobbler to cancel sky emission. The inferred average HDO production rate for the period 14 March to 8 April 2013 is $Q_{\rm HDO} = 13 \pm 3 \times 10^{26}$ molec s^{-1}, yielding $D/H = 6.5 \pm 1.6 \times 10^{-4}$. This is four times the Earth value (VSMOW $D/H = 1.56 \times 10^{-4}$), the highest value found in a comet, but compatible with the Earth value at the 3σ level.

5.2.2. D/H ratio in comet C/2014 Q2 (Lovejoy)

The tracking of the comet activity via monitoring of the CH_3OH production rate and the precise determination of the water outgassing rate using OH, $H_2^{16}O$ and $H_2^{18}O$ make us confident that we have a good H_2O production rate reference in order to derive the D/H ratio. We report here the detection of HDO with the IRAM 30 m telescope in this comet. The HDO (2_{11}−2_{12}) line was observed on 13, 15, 16, 23, and 24 January 2015. The average yields a 4σ detection (Fig. 3) corresponding to $Q_{\rm HDO} = 15.3 \pm 4.1 \times 10^{25}$ molec s^{-1}, hence a D/H ratio of $1.4 \pm 0.4 \times 10^{-4}$. Although the detection is marginal, in the worse case taking a 5σ upper limit would yield $D/H < 1.86 \times 10^{-4}$, suggesting that comet Lovejoy has a D/H ratio for water similar

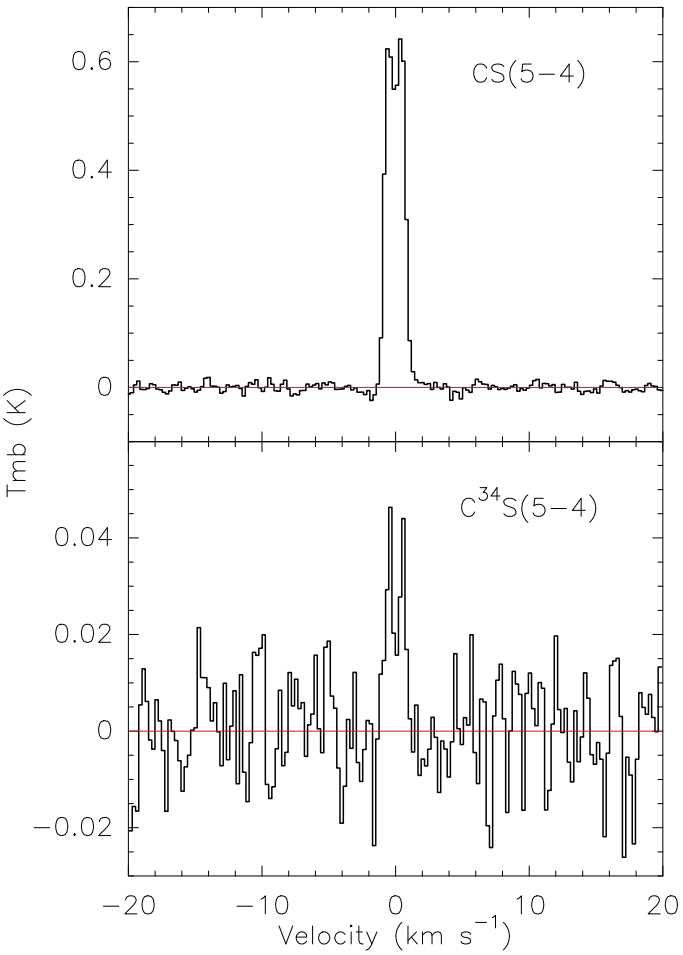

Fig. 7. Comet C/2014 Q2 (Lovejoy): average on-nucleus spectra of the CS (5−4) line at 244.936 GHz and $C^{34}S$ (5−4) line at 241.016 GHz obtained with the IRAM 30 m telescope on 13−24 January 2015. Vertical scale is main beam brightness temperature and horizontal scale Doppler velocity in the comet rest frame.

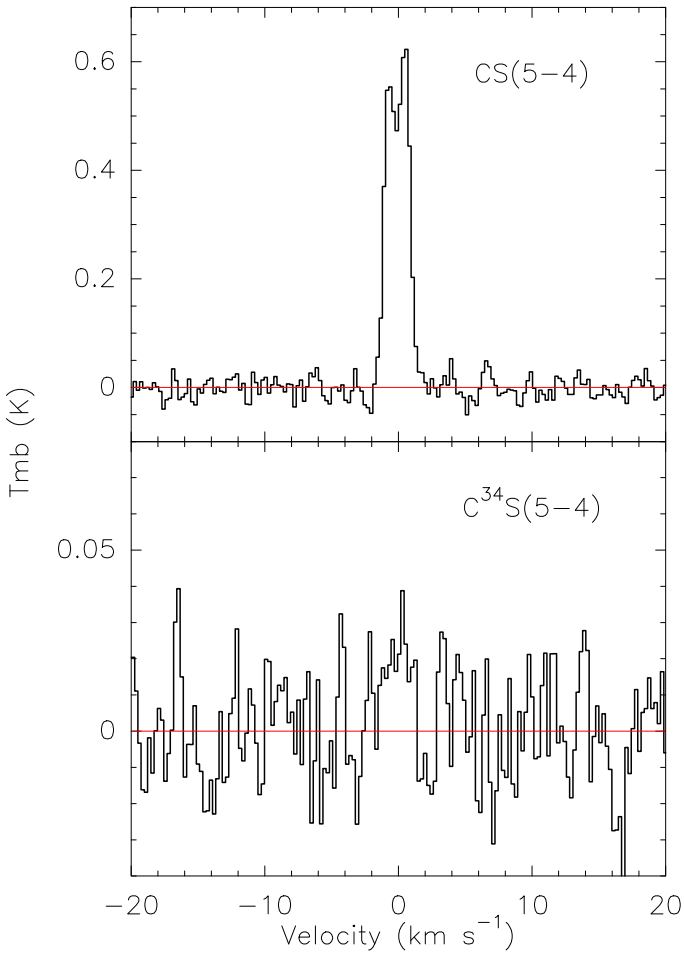

Fig. 8. Comet C/2012 F6 (Lemmon): average on-nucleus spectra of the CS (5−4) line at 244.936 GHz and $C^{34}S$ (5−4) line at 241.016 GHz obtained with the IRAM 30 m telescope between 14 March and 8 April 2013. Vertical scale is main beam brightness temperature and horizontal scale Doppler velocity in the comet rest frame.

to that of the Earth (VSMOW $D/H = 1.56 \times 10^{-4}$), or possibly even lower. Previous measurements of the D/H ratio in Oort cloud comets yielded values larger than VSMOW (see Sect. 6.1).

5.3. $^{14}N/^{15}N$ ratio in HCN

One of the primary goals of the observing program of comet Lovejoy was to measure the $^{14}N/^{15}N$ ratio in HCN. On January 13, 15, and 16 we first observed the main isotopologue transition HCN (3−2) at 265.886 GHz, then carried out longer integrations using the setup covering the $H^{13}CN$ (3−2) line at 259.012 GHz and the $HC^{15}N$ (3−2) line at 258.157 GHz (Fig. 5).

The HCN reference production rate was computed taking opacity effects into account. The average value for the 13−16 January period is $Q_{HCN} = 4.87 \pm 0.02 \times 10 \times 10^{26}$ molec s^{-1}, using pointing at the nucleus and at 5−8″ offsets – which both yield exactly the same value. The HCN production rate based on the hyperfine component HCN ($J = 3-2$, $F = 2-2$) with a total statistical weight of 3.7% is marginally higher (+14%, 2σ), possibly because of contamination by the wings of the main HCN hyperfine components.

In order to minimize biases due to time variation of the outgassing and other observing uncertainties (calibration, pointing uncertainty, etc.), we rescaled the HCN production rate to the time when $H^{13}CN$ (3−2) and $HC^{15}N$ (3−2) were observed, using the CH_3OH production rate as a reference since several methanol lines were observed in each setup. The correction applied to Q_{HCN} is +10% for the 13–16 January observations and +27% for 23–25 January. The compound $HC^{15}N$ (3−2) is clearly detected during both periods (signal-to-noise ratios of 9 and 6). The derived $^{14}N/^{15}N$ ratios are 145 ± 16 and 144 ± 23, for 13–16 January and 23–25 January, respectively.

The compounds $HC^{15}N$ (3−2) and $H^{13}CN$ (3−2) were not clearly detected (Fig. 6) in comet C/2012 F6 (Lemmon), but the 2σ value or lower limit we obtained for the $^{14}N/^{15}N$ ratio in HCN ($\geq$106 or 152 ± 72) is fully compatible with values found in other comets.

5.4. $^{12}C/^{13}C$ ratio

The $H^{13}CN$ (3−2) line at 259.012 GHz is in the same spectral band as $HC^{15}N$ (3−2). The production rates (assuming the same photo-dissociation lifetime as for HCN) and relative abundances are derived in the same way for both molecules. Owing to its hyperfine structure similar to that of $H^{12}CN$ (3−2) (Fig. 5), the $H^{13}CN$ (3−2) line only contains 93% of the flux in the (−1.2−1.2 km s^{-1}) window and this was taken into account.

The derived $^{12}C/^{13}C$ ratios in comet Lovejoy and Lemmon are 109 ± 14 and 124 ± 64, respectively. Within the uncertainties,

they are compatible with the terrestrial value (89.7) although slightly higher (1.4σ for Lovejoy). This trend was also observed for comet 17P/Holmes (Bockelée-Morvan et al. 2008) and Hale-Bopp (Jewitt et al. 1997). Combining the three $^{12}C/^{13}C$ measurements yields a value 2.5σ larger than the Earth value. This interesting result needs to be further investigated in other comets.

The sensitivity was not sufficient to detect other ^{13}C isotopologues. The most sensitive limit was reached for the $^{13}CH_3OH$ ($5_{+2}-4_{+1}E$) and $^{12}CH_3OH$ ($5_{+2}-4_{+1}E$) lines at 261.113 and 266.838 GHz, respectively. The derived lower limit is $^{12}C/^{13}C$ >61 in comet Lovejoy, compatible with the Earth value.

5.5. $^{32}S/^{34}S$ ratio

The wide 8 GHz frequency coverage of the EMIR receiver at IRAM, allows us to observe both $C^{32}S$ and $C^{34}S$ or $H_2^{32}S$ and $H_2^{34}S$ lines in the same FTS spectrum since they are less than 4 GHz apart. As a consequence, the isotopic ratios do not depend on any calibration or pointing effects and, since the lines are mostly optically thin, the abundance ratio is very close to the line intensity ratio. The integration time on the H_2S lines (either around 168 or 216 GHz) was not sufficient to yield a significant constraint on the $H_2^{32}S/H_2^{34}S$ ratio. On the other hand, the $C^{34}S$ (5–4) line at 241 016.089 MHz was detected in both comets (Figs. 7 and 8). The accuracy of the $^{32}S/^{34}S$ ratio in CS is given by the signal-to-noise ratio of the $C^{34}S$ line, and we found $^{32}S/^{34}S = 20 \pm 5$ and 24.7 ± 3.5 in comets Lemmon and Lovejoy, respectively. We do not find any significant departure from the Earth value of $^{32}S/^{34}S = 22.5$. The $C^{33}S$ line lies between the $C^{34}S$ and $C^{32}S$ lines. The upper limit for the $C^{33}S$ (5–4) line at 242.913 GHz in comet Lovejoy yields $^{32}S/^{33}S > 50$. This is the first reported estimate of ^{33}S in a comet, but this is only a lower limit compatible with the Earth value (126.7).

6. Discussion

We measured a terrestrial value for the $^{16}O/^{18}O$ ratio in water in comet Lovejoy, as was the case in all comets in which this ratio had been measured before (Balsiger et al. 1995; Biver et al. 2007; Bockelée-Morvan et al. 2012, 2015; Altwegg et al. 2015).

The D/H and $^{14}N/^{15}N$ ratios in solar system bodies are of particular importance as they vary from object to object, with the heavier elements enriched in the Earth and small bodies compared to Jupiter or the protosolar values. These ratios trace the various enrichment and fractionation mechanisms that were at play in the proto-planetary nebula. The other isotopic ratios investigated here do not show significant variations in solar system objects within the accuracy of our measurements. Figure 9 shows the $^{14}N/^{15}N$ versus D/H ratios measured in solar system objects, including our new measurements presented here.

6.1. Earth-like water in comet Lovejoy

We obtained a measurement or at least a stringent upper limit for the D/H ratio in water of two dynamically old Oort cloud comets. We measured the lowest D/H ratio in water in a comet so far: $1.4 \pm 0.4 \times 10^{-4}$ ($<1.8 \times 10^{-4}$; 5σ) in Lovejoy, while the corresponding ratio could be four times higher in comet Lemmon. These two D/H measurements are based on the same line in two comets of similar activity. Comet Lemmon was slightly more active but also two times farther away. We do not expect that the excitation mechanism of HDO in the coma of these comets

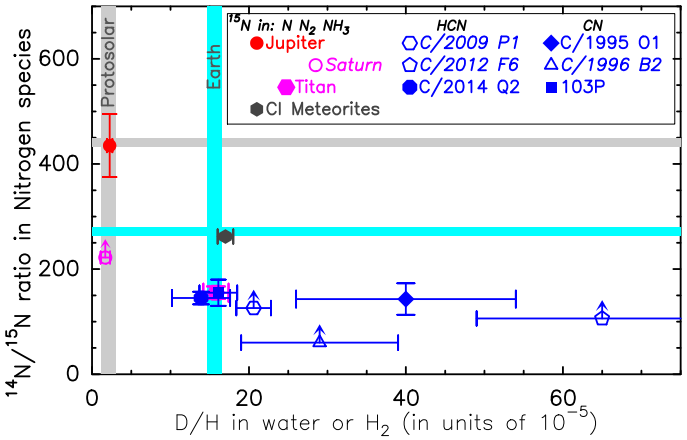

Fig. 9. D/H ratios and $^{14}N/^{15}N$ ratios in solar system objects, compared to the protosolar (gray bands) and Earth (blue bands) values (Robert et al. 2000; Marty et al. 2011). Jupiter and Saturn values are from Marty et al. (2011), Füri & Marty (2015), and Fletcher et al. (2014); Titan values from Abbas et al. (2010), Niemann et al. (2010), and Mandt et al. (2009, 2014); meteorites from Waite et al. (2009) and Kerridge (1985); and comet values from Bockelée-Morvan et al. (1998), Meier et al. (1998), Crovisier et al. (2004a), Hartogh et al. (2011), Bockelée-Morvan et al. (2012), Bockelée-Morvan et al. (2008), Hutsemékers et al. (2009), Meech et al. (2011), and this paper. The symbols corresponding to each source are given in the enclosed legend box. They are ordered according to the species in which the $^{14}N/^{15}N$ was measured from left to right: atomic nitrogen, N_2 (as for Earth), ammonia, HCN, and CN. Empty symbols with names in italics are for lower limits on the $^{14}N/^{15}N$.

can yield a factor of four difference in the derived production rates. So the observed diversity in the D/H ratio can be real and would suggest that these two comets, although they come from the same current reservoir, were formed in different places or at different times in the young solar system. In either case, this brings additional proof that comet dynamical origin does not imply a specific formation region in the disk. Previous studies (Hartogh et al. 2011; Lis et al. 2013; Bockelée-Morvan et al. 2012; Altwegg et al. 2015) have shown a growing diversity in the measured values of the D/H ratio in cometary water, and especially variations by more than a factor of 3 among Jupiter family comets, which are thought to originate from the Kuiper belt. Now we find that a similar range of values is present among Oort cloud comets. This is in line with the latest models (Brasser & Morbidelli 2013), which suggest that all comets were formed in the same extended massive original Kuiper Belt beyond the giant planets and were later scattered to the two current reservoirs, the scattered Kuiper disk and the Oort cloud. The diversity in deuterium enrichment would occur because the presolar cloud was initially enriched in HDO (higher D/H in water than in H_2: protosolar D/H value in H_2 is 2×10^{-5}, Fig. 9), but the inner warmer parts of the proto-planetary nebula lost more of their initial enrichment in deuterated water.

6.2. $^{14}N/^{15}N$ in comets

Measurements of $^{14}N/^{15}N$ in comets are relatively scarce. Although the $^{14}N/^{15}N$ ratio is 5–20 times lower than the $H_2^{16}O$ /HDO ratio, the nitrogen bearing molecules in cometary comae are less than 1% in abundance relative to water. So the detection of ^{15}N isotopologues requires very active comets. The most sensitive technique is optical high resolution spectroscopy, which has provided several detections of $C^{15}N$ (Manfroid et al. 2005, 2009; Hutsemékers et al. 2009) and recently detections

of $^{15}NH_2$ (Rousselot et al. 2014; Shinnaka et al. 2015), but this technique only gives access to daughter species. The compounds N_2 and NH_3 are not very abundant (Rubin et al. 2015; Biver et al. 2012) and do not have strong lines observable from the ground, nor do their ^{15}N isotopologues. Only HCN is easily detectable in the radio and infrared. We report here the third clear ($S/N > 10$) detection of $HC^{15}N$ in a comet after its detection in comets Hale-Bopp and 17P/Holmes (Bockelée-Morvan et al. 2008).

We measure the same enrichment in ^{15}N in HCN in comet Lovejoy as in other comets, in spite of their different dynamical origins (Bockelée-Morvan et al. 2008). The same enrichment was also found in CN in many other comets (Hutsemékers et al. 2009). This is a factor of two enrichment in ^{15}N in comparison to the Earth atmospheric value (272) and a factor of three in comparison to the proto-planetary value (441, Marty et al. 2011) (Fig. 9). The enrichment is similar to that found in NH_2 (Rousselot et al. 2014; Shinnaka et al. 2015), thought to be mostly produced by the photo-dissociation of NH_3, the main volatile carrier of cometary nitrogen (Biver et al. 2012).

Correspondingly low $^{14}N/^{15}N$ ratios are also detected in carbonaceous interplanetary dust particles (IDPs) (Messenger 2000; Floss et al. 2004). These large enrichments with respect to solar or terrestrial values can be explained by interstellar chemistry theories involving ion-molecule ^{15}N fractionation at 10 K (e.g., Wirström et al. 2012). Recently, significant nitrogen fractionation has been measured in dark cloud cores with ratios as low as 150 for nitriles (Milam et al. 2015). Thus, the similarity of the $^{14}N/^{15}N$ ratios found in comets and IDPs strengthens a putative link to interstellar chemistry as the origin of isotopically anomalous organic particles in comets.

Nevertheless, our observations confirms that the trend of a twofold enrichment in ^{15}N compared to Earth observed in $C^{15}N$ is also present in HCN. A consequence concerning the debate of the origin of CN in cometary coma is that we cannot exclude HCN as the sole parent of CN on the basis of different $^{14}N/^{15}N$ ratios.

7. Conclusions

Chemical diversity is observed in the population of Oort Cloud comets, with abundances varying by up to a factor of ten for several species. The origin of this diversity is unclear and might reflect comet formation at different places or times in the early solar system.

The observations presented here provide further evidence that diversity is present in the enrichment in deuterium in cometary water with respect to the protosolar value (HD/H_2), both in Jupiter family and Oort cloud comets, in line with the latest scenarios of comet origins (Brasser & Morbidelli 2013). On the one hand, we found Earth-like D/H, $^{16}O/^{18}O$, $^{12}C/^{13}C$, and $^{32}S/^{34}S$ ratios in comet C/2014 Q2 (Lovejoy), strengthening the role that some comets may have played in supplying material to the young Earth, especially complex organic molecules (Biver et al. 2015). On the other hand we confirm the trend of finding a systematic twofold enrichment in ^{15}N in cometary HCN relative to its abundance in Earth N_2, whose origin is puzzling.

We were also able to obtain in comet C/2014 Q2 sensitive limits, some of the best obtained so far with remote observations, on isotopic ratios in other molecules such as D/H in H_2S, H_2CO, or $C^{32}S/C^{33}S$.

Acknowledgements. The IRAM observations were conducted under the target of opportunity proposal D04-14 and regular proposal 128-14 and we gratefully acknowledge the support from the IRAM director for awarding us discretionary time and the IRAM staff for its support and for scheduling the observations on short notice. This research has been supported by the Programme national de planétologie de l'Institut des sciences de l'univers (INSU). S.N.M. acknowledges the NASA Planetary Astronomy program for support.

References

Abbas, M. M., Kandadi, H., LeClair, A., et al. 2010, ApJ, 708, 342
Altwegg, K., & Bockelée-Morvan, D. 2003, Space Sci. Rev., 106, 139
Altwegg, K., Balsiger, H., Bar-Nun, A., et al. 2015, Science, 347, 1261952
Balsiger, H., Altwegg, K., & Geiss, J. 1995, J. Geophys. Res., 100, 5827
Biver, N., Bockelée-Morvan, D., Crovisier, J., et al. 2000, AJ, 120, 1554
Biver, N., Bockelée-Morvan, D., Crovisier, J., et al. 2006, A&A, 449, 1255
Biver, N., Bockelée-Morvan, D., Crovisier, J., et al. 2007, Planet. Space Sci., 55, 1058
Biver, N., Crovisier, J., Bockelée-Morvan, D., et al. 2012, A&A, 539, A68
Biver, N., Bockelée-Morvan, D., Debout, V., et al. 2014, A&A, 566, L5
Biver, N., Bockelée-Morvan, D., Moreno, R., et al. 2015, Sci. Adv., 1, e1500863
Bockelée-Morvan, D., Gautier, D., Lis, D. C., et al. 1998, Icarus, 133, 147
Bockelée-Morvan, D., Lis, D. C., Wink, J. E., et al. 2000, A&A, 353, 1101
Bockelée-Morvan, D., Biver, N., Jehin, E., et al. 2008, ApJ, 679, L49
Bockelée-Morvan, D., Biver, N., Swinyard, B., et al. 2012, A&A, 544, L15
Bockelée-Morvan, D., Calmonte, U., Charnley, S., et al. 2015, Space Sci. Rev., 197, 47
Brasser, R., & Morbidelli, A. 2013, Icarus, 225, 40
Carter, M., Lazareff, R., Maier, D., et al. 2012, A&A, 538, A89
Combi, M. R., Bertaux, J.-L., Quémerais, E., et al. 2014, AJ, 147, 126
Crovisier, J. 1994, J. Geophys. Res., 99, 3777
Crovisier, J., Bockelée-Morvan, D., Biver, N., et al. 2004a, A&A, 418, L35
Crovisier, J., Bockelée-Morvan, D., Colom, P., et al. 2004b, A&A, 418, 1141
Fletcher, L. N., Greathouse, T. K., Orton, G. S., et al. 2014, Icarus, 238, 170
Floss, C., Stadermann, F. J., Bradley, J., et al. 2004, Science, 303, 1355
Frisk, U., Hagström, M., Ala-Laurinaho, J., et al. 2003, A&A, 402, L27
Füri, E., & Marty B. 2015, Nature Geoscience, 8, 515
Gérard, E., Crovisier, J., Colom, P., et al. 1998, Planet. Space Sci., 46, 569
Hartogh, P., Lis, D. C., Bockelée-Morvan, D., et al. 2011, Nature, 478, 218
Hutsemékers, D., Manfroid, J., Jehin, E., & Arpigny, C. 2009, Icarus, 204, 346
Jewitt, D., Matthews, H. E., Owen, T., & Meier, R. 1997, Science, 278, 90
Kerridge, J. F. 1985, Geochim. Cosmochim. Acta, 49, 1707
Lis, D. C., Biver, N., Bockelée-Morvan, D., et al. 2013, ApJ, 774, L3
Mandt, K. E., Waite, J. H., Lewis, W., et al. 2009, Planet. Space Sci., 57, 1917
Mandt, K. E., Mousis, O., Lunine, J., & Gautier, D. 2014, ApJ, 788, L24
Manfroid, J., Jehin, E., Hutsemékers, D., et al. 2005, A&A, 432, L5
Manfroid, J., Jehin, E., Hutsemékers, D., et al. 2009, A&A, 503, 613
Marty, B., Chaussidon, M., Wiens, R. C., Jurewicz, A. J. G., & Burnett, D. S. 2011, Science, 332, 1533
Meech, K. J., A'Hearn, M. F., Adams, J. A., et al. 2011, ApJ, 734, L1
Meier, R., Owen, T. C., Matthews, H. E., et al. 1998, Science, 279, 842
Messenger, S. 2000, Nature, 404, 968
Milam, S. N., Adande, G., Cordiner, M. A., Wirstrom, E., & Charnley, S. B. 2015, LPI Contribution, 1832, 1934
Müller, H. S. P., Schlöder, F., Stutzki J., & Winnewisser, G. 2005, J. Mol. Struct., 742, 215
Niemann, H. B., Atreya, S. K., Demick, J. E., et al. 2010, J. Geophys. Res., 115, E12, E12006
O'Brien, D. P., Walsh, K. J., Morbidelli, A., Raymond, S. N., & Mandell, A. M. 2014, Icarus, 239, 74
Paganini, L., DiSanti, M. A., Mumma, M. J., et al. 2014, AJ, 147, 15
Pickett, H. M., Poynter, R. L., Cohen, E. A., et al. 1998, J. Quant. Spectr. Rad. Transf., 60, 883
Robert, F., Gautier, D., & Dubrulle, B. 2000, Space Sci. Rev., 92, 201
Rousselot, P., Pirali, O., Jehin, E., et al. 2014, ApJ, 780, L17
Rubin, M., Altwegg, K., Balsiger, H., et al. 2015, Science, 348, 232
Shinnaka, Y., Kawakita, H., Kobayashi, H., et al. 2015, ApJ, 782, L16
Waite, J. H., Jr., Lewis, W. S., Magee, B. A., et al. 2009, Nature, 460, 487
Wirström, E. S., Charnley, S. B., Cordiner, M. A., & Milam, S. N. 2012, ApJ, 757, L11
Zakharov, V., Bockelée-Morvan, D., Biver, N., Crovisier, J., & Lecacheux, A. 2007, A&A, 473, 303

Appendix A: Additional tables

Table A.1. Circumstances of IRAM observations and reference parameters.

UT date (yyyy/mm/dd.d–dd.d)	$\langle r_h \rangle$ (AU)	$\langle \Delta \rangle$ (AU)	Integ. time (min)[a]	Freq. range (GHz)	v_{exp} (km s^{-1})	T_{kin} (K)	Q_{H_2O}[b,c] (molec s^{-1})	Q_{CH_3OH} (molec s^{-1})
Comet C/2012 F6 (Lemmon):								
2013/03/14.52–14.55	0.758	1.348	26	249-256, 264-272	1.10	110	$\sim 10 \times 10^{29}$	$2.1 \pm 0.1 \times 10^{28}$
2013/03/14.57–14.59	0.758	1.349	20	240-248, 256-264	1.10	110	$\sim 10 \times 10^{29}$	$2.3 \pm 0.1 \times 10^{28}$
2013/03/15.52–15.57	0.753	1.362	21	249-256, 264-272	1.10	110	$\sim 10 \times 10^{29}$	$1.7 \pm 0.2 \times 10^{28}$
2013/03/15.58–15.59	0.753	1.362	14	210-218, 226-234	1.10	110	$\sim 10 \times 10^{29}$	
2013/03/18.53–18.55	0.741	1.400	17	249-256, 264-272	1.10	110	$\sim 10 \times 10^{29}$	$1.6 \pm 0.2 \times 10^{28}$
2013/03/18.55–18.59	0.741	1.400	20	240-248, 256-264	1.10	110	$\sim 10 \times 10^{29}$	$2.1 \pm 0.1 \times 10^{28}$
2013/04/06.40–06.51	0.776	1.592	69	249-256, 264-272	1.00	100	$\sim 9 \times 10^{29}$	$1.5 \pm 0.1 \times 10^{28}$
2013/04/06.53–06.60	0.776	1.592	54	240-248, 256-264	1.00	100	$\sim 9 \times 10^{29}$	$1.4 \pm 0.1 \times 10^{28}$
2013/04/07.49–07.52	0.783	1.600	20	249-256, 264-272	1.00	100	$\sim 9 \times 10^{29}$	$1.6 \pm 0.2 \times 10^{28}$
2013/04/07.53–07.59	0.783	1.600	58	210-218, 226-234	1.00	100	$\sim 9 \times 10^{29}$	$1.2 \pm 0.4 \times 10^{28}$
2013/04/08.43–08.50	0.790	1.606	62	85-93, 166-170	1.00	100	$\sim 9 \times 10^{29}$	$1.5 \pm 0.1 \times 10^{28}$
2013/04/08.51–08.54	0.790	1.606	28	249-256, 264-272	1.00	100	$\sim 9 \times 10^{29}$	$1.5 \pm 0.1 \times 10^{28}$
2013/04/08.55–08.59	0.791	1.607	36	218-226, 234-242	1.00	100	$\sim 9 \times 10^{29}$	$1.7 \pm 0.2 \times 10^{28}$
Comet C/2014 Q2 (Lovejoy):								
2015/01/13.75–13.77	1.314	0.496	14	249-256, 264-272	0.80	73	5×10^{29}	$1.17 \pm 0.03 \times 10^{28}$
2015/01/13.79–13.84	1.314	0.497	29	210-218, 225-233	0.80	73	5×10^{29}	$1.25 \pm 0.07 \times 10^{28}$
2015/01/13.85–13.88	1.313	0.497	29	240-248, 256-264	0.80	73	5×10^{29}	$1.25 \pm 0.02 \times 10^{28}$
2015/01/15.82–15.83	1.308	0.516	13	249-256, 264-272	0.80	73	5×10^{29}	$1.18 \pm 0.04 \times 10^{28}$
2015/01/15.85–15.96	1.308	0.516	105	240-248, 256-264	0.80	73	5×10^{29}	$1.42 \pm 0.02 \times 10^{28}$
2015/01/16.76–16.78	1.306	0.526	14	249-256, 264-272	0.80	73	5×10^{29}	$1.14 \pm 0.01 \times 10^{28}$
2015/01/16.81–16.95	1.306	0.527	120	240-248, 256-264	0.80	73	5×10^{29}	$1.17 \pm 0.02 \times 10^{28}$
2015/01/23.72–23.75	1.294	0.624	36	240-248, 256-264	0.80	73	6×10^{29}	$1.48 \pm 0.03 \times 10^{28}$
2015/01/24.73–24.75	1.293	0.641	14	226-234, 241-249	0.80	73	6×10^{29}	$1.27 \pm 0.06 \times 10^{28}$
2015/01/25.71–25.75	1.292	0.658	42	210-218, 225-233	0.80	73	6×10^{29}	$1.00 \pm 0.04 \times 10^{28}$
2015/01/26.74–26.75	1.291	0.675	6	85-93, 101-109	0.80	73	7×10^{29}	$1.99 \pm 0.20 \times 10^{28}$

Notes. [a] On nucleus pointings only. [b] For comet Lemmon, Combi et al. (2014) provide Q_{H_2O} values in the range $7-12 \times 10^{29}$ molec s^{-1} during this period. Contemporaneous SWAN measurements are slightly lower than quoted here, but they were not time-deconvolved and the average values measured by SWAN a few days later are within 10% of those given here. Given our measured Q_{CH_3OH} (Col. 9), Q_{H_2O} are also in agreement with the measurement of Paganini et al. (2014) as they yield the same Q_{CH_3OH}/Q_{H_2O} ratio. Nançay observations are also compatible with these Q_{H_2O} although the quenching of the OH maser is poorly constrained and the uncertainty on Q_{OH} is very large. [c] For comet Lovejoy, Q_{H_2O} are based on *Odin* and Nançay data (see text and Biver et al. 2015).

Table A.2. Line intensities from IRAM observations and production rates.

Date [yyyy/mm/dd.d – dd.d]	Molecule	Transition	Frequency [MHz]	Intensity [mK km s^{-1}]	Total production rate [10^{26} molec. s^{-1}]
Comet C/2012 F6 (Lemmon) March-April 2013					
2013/03/14.5-18.6	HCN	3–2	265 886.432	6055 ± 36	15.3 ± 2.1[a]
2013/04/06.46	HCN	3–2		5966 ± 50	13.1 ± 0.8[a]
2013/03/14.5-18.6	H^{13}CN	3–2	259 011.798	65 ± 44	<0.28
2013/04/06.56	H^{13}CN	3–2		43 ± 32	<0.20
2013/03/14.5-37.6	H^{13}CN	3–2		51 ± 26	0.12 ± 0.06
2013/03/14.5-18.6	HC^{15}N	3–2	258 156.996	108 ± 36	<0.25
2013/04/06.46	HC^{15}N	3–2		11 ± 22	<0.14
2013/03/14.5-37.6	HC^{15}N	3–2		40 ± 19	0.09 ± 0.04
2013/03/15.6-38.6	DCN	3–2	217 238.538	<133	<0.52
2013/04/08.47	H_2S	$1_{10}-1_{01}$	168 762.762	234 ± 36	77 ± 13[a]
2013/04/08.47	$H_2^{34}S$	$1_{10}-1_{01}$	167 910.516	<66	<21
2013/03/14.6-18.6	CS	5–4	244 935.557	1477 ± 38	14.7 ± 0.6[a]
2013/04/06.56	CS	5–4		1019 ± 25	9.5 ± 0.2
2013/03/14.6-18.6	C^{34}S	5–4	241 016.089	50 ± 31	0.51 ± 0.31
2013/04/06.56	C^{34}S	5–4		58 ± 16	0.57 ± 0.16
2013/03/15.6-38.6	C^{34}S	5–4		53 ± 13	0.54 ± 0.13
2013/03/14.6-18.6	HDO	$2_{11}-2_{12}$	241 561.550	88 ± 29	21 ± 7
2013/04/06.56	HDO	$2_{11}-2_{12}$		44 ± 19	12 ± 4
2013/03/14.6-37.6	HDO	$2_{11}-2_{12}$		54 ± 14	13 ± 3
Comet C/2014 Q2 (Lovejoy) 13–25 January 2015					
2015/01/13.7-16.8	HCN	3–2	265 886.432	10848 ± 39	4.9 ± 0.2[a]
2015/01/13.7-16.8	H^{13}CN	3–2	259 011.798	114 ± 13	0.049 ± 0.006
2015/01/23.73	H^{13}CN	3–2		86 ± 18	0.043 ± 0.009
2015/01/13.7-23.7	H^{13}CN	3–2		100 ± 12	0.046 ± 0.006
2015/01/13.7-16.8	HC^{15}N	3–2	258 156.996	86 ± 9	0.037 ± 0.004
2015/01/23.73	HC^{15}N	3–2		85 ± 13	0.043 ± 0.007
2015/01/13.7-23.7	HC^{15}N	3–2		83 ± 7	0.039 ± 0.003
2015/01/13.7-24.7	DCN	3–2	217 238.538	<39	<0.031
2015/01/13.7-16.8	CH_3OH	5_2-4_1E	266 838.123	1345 ± 24	117 ± 3[a]
2015/01/13.7-23.7	$^{13}CH_3OH$	5_2-4_1E	263 113.343	<23	<2.4
2015/01/13.7-25.7	H_2CO	$3_{13}-2_{12}$	211 211.469	978 ± 11	18 ± 1[a]
2015/01/13.7-25.7	H_2CO	$3_{12}-2_{11}$	225 697.772	1181 ± 17	18 ± 1[a]
2015/01/13.7-23.7	HDCO	$4_{14}-3_{13}$	246 924.600	<18	<0.38
2015/01/13.7-23.7	HDCO	$4_{04}-3_{03}$	256 585.531	<21	<0.36
2015/01/13.8-25.7	H_2S	$2_{20}-2_{11}$	216 710.437	227 ± 12	17.3 ± 0.9[a]
2015/01/13.8-25.7	$H_2^{34}S$	$2_{20}-2_{11}$	214 376.924	16 ± 11	<2.6
2015/01/13.8-23.7	HDS	$2_{11}-2_{02}$	257 781.410	<21	<0.6
2015/01/13.8-16.9	CS	5–4	244 935.557	1049 ± 10	2.14 ± 0.02[a]
2015/01/23.7-24.7	CS	5–4		1089 ± 10	2.51 ± 0.02[a]
2015/01/13.8-23.7	CS	5–4		1076 ± 7	2.30 ± 0.02[a]
2015/01/13.8-16.9	C^{34}S	5–4	241 016.089	37 ± 9	0.077 ± 0.019
2015/01/23.73	C^{34}S	5–4		53 ± 13	0.126 ± 0.031
2015/01/13.8-23.7	C^{34}S	5–4		42 ± 6	0.093 ± 0.013
2015/01/13.8-23.7	C^{33}S	5–4	242 913.610	<21	<0.046
2015/01/13.8-16.9	HDO	$2_{11}-2_{12}$	241 561.550	31 ± 8	1.8 ± 0.4
2015/01/23.7-24.7	HDO	$2_{11}-2_{12}$		23 ± 11	1.6 ± 0.7
2015/01/13.8-24.7	HDO	$2_{11}-2_{12}$		25 ± 7	1.5 ± 0.4

Notes. [(a)] Average production rate for the period also taking into account measurements at 5 to 20″ offsets. For formaldehyde the offset positions were used to constrain the contribution of the distributed source: 80% with a scale-length of 10 000 km.